



# A novel wireless optical technique for quantitative evaluation of cerebral perfusion pressure in a fluid percussion animal model of traumatic brain injury

Yao-Kuang Huang<sup>1,2^</sup>, Chin-Kuo Lin<sup>2,3</sup>, Che-Chuan Wang<sup>4</sup>, Jinn-Rung Kuo<sup>4</sup>, Chien-Fu Lai<sup>5</sup>, Chien-Wei Chen<sup>1,2</sup>, Bor-Shyh Lin<sup>5^</sup>

<sup>1</sup>Division of Cardiovascular Surgery and Radiology, Chiayi Chang Gung Memorial Hospital, Putz, Chiayi; <sup>2</sup>College of Medicine, Chang Gung University, Taoyuan; <sup>3</sup>Division of Pulmonary Infection and Critical Care, Department of Pulmonary and Critical Care Medicine, Chiayi Chang Gung Memorial Hospital, Putz, Chiayi; <sup>4</sup>Division of Neurosurgery, Department of Surgery, Chi Mei Medical Center, Tainan; <sup>5</sup>Institute of Imaging and Biomedical Photonics, National Yang Ming Chiao Tung University, Tainan

*Correspondence to:* Bor-Shyh Lin, PhD. Institute of Imaging and Biomedical Photonics, National Chiao Tung University, Tainan.  
Email: borshyhlin@gmail.com.

**Background:** Cerebral perfusion pressure (CPP) calculated by mean arterial pressure (MAP) minus intracranial pressure (ICP) is related to blood flow into the brain and reflects cerebral ischemia and oxygenation indirectly. Near-infrared spectroscopy (NIRS) can assess cerebral ischemia and hypoxia non-invasively and has been widely used in neuroscience. However, the correlation between CPP and NIRS, and its potential application in traumatic brain injury, has seldom been investigated.

**Methods:** We used a novel wireless NIRS system and commercial ICP and MAP devices to assess the trauma to rat brains using different impact intensity. The relationship between CPP and NIRS parameters with increasing impact strength were investigated.

**Results:** The results showed that changes in CPP ( $\Delta$ CPP), oxy-hemoglobin [ $\Delta$ [HbO<sub>2</sub>]], total-hemoglobin [ $\Delta$ [HbT]], and deoxy-hemoglobin were inversely proportional to the increase in impact intensity, and the correlations between  $\Delta$ CPP, NIRS parameters [ $\Delta$ [HbO<sub>2</sub>]], and [ $\Delta$ [HbT]] were significant.

**Conclusions:** The NIRS system can assess cerebral ischemia and oxygenation non-invasively and changes of HbO<sub>2</sub> and HbT may be used as reference parameters to assess the level of CPP in an animal model of traumatic brain injury.

**Keywords:** Near-infrared spectroscopy (NIRS); oxy-hemoglobin (HbO<sub>2</sub>); deoxy-hemoglobin; total-hemoglobin (HbT); cerebral perfusion pressure (CPP); traumatic brain injury (TBI)

Submitted Jun 18, 2020. Accepted for publication Jan 18, 2021.

doi: 10.21037/qims-20-777

View this article at: <http://dx.doi.org/10.21037/qims-20-777>

## Introduction

Traumatic brain injuries (TBIs) are usually caused by falls, vehicle accidents, and assault, and result in significant death and disability worldwide. The outcome of TBIs can be

divided into primary and secondary brain injury. Primary brain injury occurs at the moment external forces, such as direct collision, acceleration or deceleration, or rotational forces, are exerted on the brain. Since primary brain injury

<sup>^</sup> ORCID: Yao-Kuang Huang, 0000-0003-2699-2207; Bor-Shyh Lin, 0000-0002-8653-2571.

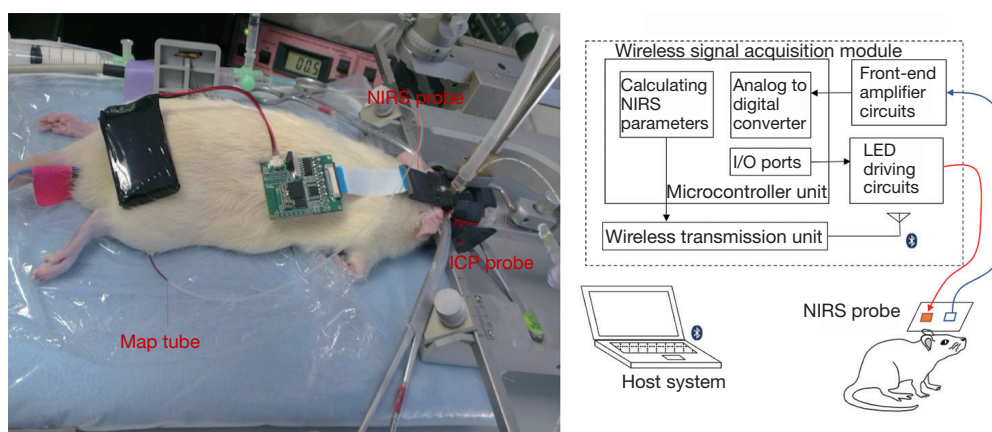


**Figure 1** Photographs of the MAP/ICP experiment (left side) and module (right side) in this study. NIRS, near-infrared spectroscopy; ICP, intracranial pressure; MAP, mean arterial pressure; LED, light emitting diode.

occurs so rapidly, it is difficult to prevent and probably leads to secondary brain injury with delayed injury occurring in the hours and days following the initial brain injury. The major causes of secondary brain injury include ischemia, cerebral hypoxia, and increased intracranial pressure (ICP). Therefore, the main scope of multimodality management of TBI patients admitted to the intensive care unit is to obtain a continuous multiparameter monitoring designed to minimize secondary brain injury which could lead to clinical worsening and need for surgical intervention (1-4).

Cerebral perfusion pressure (CPP) monitoring has become the gold standard in clinical practice to prevent secondary brain injury in patients with TBI. CPP, defined as the difference between mean arterial pressure (MAP) and ICP, has been reported to be associated with cerebral blood flow (CBF), and the value of CPP in critical care has been reported to indirectly reflect whether there is sufficient oxygenated blood flow into the brain. After a TBI, increased ICP causing lower CPP is the main cause of cerebral ischemia, which leads to cerebral hypoxia and has been proven to be a trigger of secondary brain injury (5). Partial pressure of brain tissue oxygen (PbtO<sub>2</sub>) monitoring is often used to evaluate cerebral oxygenation levels, and a relationship between CPP and cerebral oxygenation has been proven in previous studies. In 2005, Jaeger *et al.* showed a relationship between CPP, regional cerebral blood flow (rCBF), and PbtO<sub>2</sub> after TBI, and the change in CPP was the same as that seen in rCBF and PbtO<sub>2</sub> (6), and in 2011, Friess *et al.* found a strong correlation between CPP and PbtO<sub>2</sub> after brain injury in swine (7). However, PbtO<sub>2</sub> monitoring is an invasive process that may increase the risk of brain hemorrhage and infection, and is not

convenient in clinical practice (8).

Near-infrared spectroscopy (NIRS) is widely used in neurology to assess cerebral ischemia and cerebral hypoxia. In 1985, Ferrari *et al.* first proposed applying NIRS to human brains (9). Some pioneers indicated that NIRS could check the pathophysiology of brain injury through monitoring cerebral oxygenation and hemodynamics in diseased infants (10). NIRS has several advantages over PbtO<sub>2</sub>, including the ability to demonstrate global cerebral oxygenation, and that it is non-invasive. To address the unmet needs of TBI management the neurotraumatology community has now focused on NIRS to monitor cerebral perfusion and brain permeability (11,12). In this study, a wireless multi-channel NIRS was used to record continuous concentration changes of oxy-hemoglobin (HbO<sub>2</sub>), deoxy-hemoglobin (HbR), and total-hemoglobin (HbT) of the brain during and after TBI. Changes in CPP ( $\Delta$ CPP) during TBI were also monitored. The relationships between HbO<sub>2</sub>, HbR and HbT, and CPP under different traumatic intensity were analyzed.

## Methods

### NIRS system

A NIRS system (Figure 1) was designed and implemented to continuously monitor the relative concentrations of HbO<sub>2</sub> and HbR under TBI (13). The NIRS probe consisted of light emitting diodes (LEDs) (SMT735/850, EPITEX, Japan) and photodiodes (PDs) (PD15-22C/TR8, EVERLIGHT, Taiwan). The LEDs were used to provide 735 nm and 850 nm wavelength light sources, and the PDs were used to detect and convert the diffusely reflected

lights into electrical signals. Most of the light emitted by the LEDs will be rapidly diffused when passing through biological tissue due to scattering, and only part of the light will be absorbed by the tissue, especially HbO<sub>2</sub> and HbR, which are the main absorbers of near-infrared wavelength light. The diffusely reflected light detected by the PDs will be delivered to the wireless signal acquisition module, then amplified, filtered, digitized, and transmitted wirelessly to the host system. The power of the light source is less than 3 mW, and the sampling rate of this system is set to 25 Hz. The wireless options are particularly designed for a further awake animal model of NIRS cerebral perfusion experiment.

In general, the mean path of light is shaped like a banana, and the maximum penetrating depth is about a half of the distance between the light source and the detector (14,15). By using this rule, the specific monitoring area can be determined. The variation in the concentrations of HbO<sub>2</sub> and HbR can be quantified by modifying the Beer-Lambert law. For a specific wavelength  $\lambda$ , the variation in the concentration of absorber, such as  $\Delta[\text{HbO}_2]$  and  $\Delta[\text{HbT}]$ , will cause the change of optical intensity

$$\Delta OD(\lambda) = -\log \frac{I_f(\lambda)}{I_i(\lambda)} = (\varepsilon_{\text{HbO}_2}(\lambda)\Delta[\text{HbO}_2] + \varepsilon_{\text{HbR}}(\lambda)\Delta[\text{HbR}])B(\lambda) \quad [1]$$

where  $I_f$  and  $I_i$  denote the reflected light intensities before and after the concentration change respectively,  $B$  is the differential path length factor, and  $L$  denotes the distance between the light source and the detector. Here,  $\varepsilon_{\text{HbO}_2}$  and  $\varepsilon_{\text{HbR}}$  denote the extinction coefficients of HbO<sub>2</sub> and HbT respectively. Next, the variations in the concentrations of HbO<sub>2</sub> and HbT can be solved by using the change of the optical intensity corresponding to two or more different wavelengths

$$\Delta[\text{HbO}_2] = \frac{\varepsilon_{\text{HbR}}(\lambda_1) \frac{\Delta OD(\lambda_2)}{B(\lambda_2)} - \varepsilon_{\text{HbR}}(\lambda_2) \frac{\Delta OD(\lambda_1)}{B(\lambda_1)}}{(\varepsilon_{\text{HbR}}(\lambda_1)\varepsilon_{\text{HbO}_2}(\lambda_2) - \varepsilon_{\text{HbR}}(\lambda_2)\varepsilon_{\text{HbO}_2}(\lambda_1))L} \quad [2]$$

$$\Delta[\text{HbR}] = \frac{\varepsilon_{\text{HbO}_2}(\lambda_2) \frac{\Delta OD(\lambda_1)}{B(\lambda_1)} - \varepsilon_{\text{HbO}_2}(\lambda_1) \frac{\Delta OD(\lambda_2)}{B(\lambda_2)}}{(\varepsilon_{\text{HbR}}(\lambda_1)\varepsilon_{\text{HbO}_2}(\lambda_2) - \varepsilon_{\text{HbR}}(\lambda_2)\varepsilon_{\text{HbO}_2}(\lambda_1))L} \quad [3]$$

and the changes in total-hemoglobin can be defined as:

$$\Delta[\text{HbT}] = \Delta[\text{HbO}_2] + \Delta[\text{HbR}] \quad [4]$$

### Animal preparation

Adult male Sprague-Dawley rats (n=16), weighing 375

±25 g were used in the experiments. All rats were raised on a 12-hour light/12-hour dark cycle and allowed free access to food and water. All experimental procedures conformed to the guidelines of the National Institute of Health and were approved by the Animal Care and Use Committee of Chi-Mei Medical Center (Affidavit of approval of Animal Use Protocol, Chi-Mei medical center, IACUC Approval No. 102120603) to minimize discomfort to the animals during the surgery and recovery periods. The 16 rats were randomly assigned to four impact groups (sham, 1.6, 2.0, and 2.4 atm), and monitored by the wireless NIRS system, and ICP and MAP devices. The rats were anesthetized with sodium pentothal (25 mg/kg, i.p.; Sigma Chemical Co., St Louis, MO, USA) and a mixture containing ketamine (44 mg/kg, i.m.; Nan Kuang Pharmaceutical, Tainan, Taiwan), atropine (0.02633 mg/kg, i.m.; Sintong Chemical Industrial Co., Ltd., Taoyuan, Taiwan), and xylazine (6.77 mg /kg, i.m.; Bayer, Leverkusen, Germany), and were sacrificed on the third day post-surgery.

### Experiment design for TBI

In this study, a fluid percussion injury (FPI) model was used to reproduce TBI in the rats (16). The rats were first anesthetized and their heads then placed into a stereotaxic frame, and the ears were inserted using ear bars to secure the head. To maintain the core temperature at 37 °C, a rectal temperature probe attached to a thermostatic controller was inserted into the colon. The head fur was then trimmed, and the scalp sagittally incised. A circular craniotomy on the skull was drilled to set the impact point, which was located anterior-posteriorly -3 mm and laterally +4 mm from the bregma and a luer-lock connector with a sealed and fluid-filled reservoir was secured into the craniotomy. The wireless NIRS system, and ICP and MAP monitoring devices were then installed and monitoring was performed for two hours. A pendulum then struck the reservoir to generate a fluid wave to impact the brain, and a respiratory treatment procedure was carried out to assist the respiration of the rats immediately after the FPI experiment. Upon completion of the experiments, the monitoring devices and connector were removed, and the incisions were sutured.

The monitoring position of the NIRS probe focused on the striatum region of the brain, and the maximum penetrating depth was approximately 8 mm and located anterior-posteriorly -0.5 mm and laterally +3.5 mm from the bregma. The changes in 30-second HbO<sub>2</sub> and HbR were recorded as the data baseline before the FPI

**Table 1** Post-hoc power analysis for comparing two-group means

Group	Impact strength	HbT	HbO <sub>2</sub>	HbR	ICP	CPP
Group 2	1.6 atm	98.7%	96.6%	96.5%	58.7%	3.7%
	2.0 atm	54.6%	24.9%	53.3%	56.1%	27.0%
	2.4 atm	20.4%	7.7%	79.0%	37.0%	4.8%
Group 1	Sham					

Post-hoc power was estimated using the means and standard deviation at median-time (60 minutes) and the sample sizes per group (n=4). Impact group sham was defined as group 1. Impact group 1.6, 2.0, and 2.4 atm were defined as group 2, respectively. The significance level of alpha was defined as 0.05. HbO<sub>2</sub>, oxy-hemoglobin; HbT, total-hemoglobin; HbR, deoxy-hemoglobin; ICP, intra-cranial pressure; CPP, cerebral perfusion pressure.

experiments.

The mean arterial blood pressure was measured by cannulating the femoral artery with a 3-way stopcock connected with a pressure transducer and a data acquisition system (PowerLab/8sp, ADInstruments) was also used. In addition, a pressure-monitoring catheter to monitor ICP (Codman ICP Express Monitor, Codman & Shurtleff, Inc.) inserted anterior-posteriorly -0.8 mm and laterally +4 mm from the bregma, was installed on the stereotaxic frame. When the experiment began, the MAP and ICP data were initially recorded as the baseline. Thereafter, MAP and ICP values were recorded per 10 minutes. For recording the short-term MAP and ICP, the data during impact and 4.5 minutes after impact were also recorded (Supplementary file).

### Statistical analysis

The time courses of HbO<sub>2</sub>, HbR, HbT, CPP, and ICP at different impact strengths, and their mean values after FPI at different impact strengths were analyzed using analysis of variance. Power analysis is listed in Table 1. Significance was defined as a P value of less than 0.05 and the linear correlation coefficients between CPP and NIRS parameters were analyzed using MATLAB.

## Results

The changes in relative concentrations of HbO<sub>2</sub> {Δ[HbO<sub>2</sub>]}, HbR {Δ[HbR]}, HbT {Δ[HbT]}, CPP, and ICP during and after TBI were first investigated. Bland-Altman analysis was performed first, showing most of the measured differences within the limit of agreement (Figure 2) and the concentration changes Δ[HbO<sub>2</sub>], Δ[HbR], and Δ[HbT] during and after the different impact strengths are shown in Figure 3. The time of the impact point was set at

0.5 minutes, and the respiratory treatment was carried out within 1 minute after the impact to help with spontaneous respiration. The experimental results showed that Δ[HbO<sub>2</sub>], Δ[HbR], and Δ[HbT] dropped immediately at the impact point and then rose rapidly after the respiratory treatment. The trends of Δ[HbO<sub>2</sub>], Δ[HbR], and Δ[HbT] were inverted to the increased impact intensity. Moreover, Δ[HbO<sub>2</sub>] and Δ[HbT] corresponded to the different impact intensity significantly. While after the FPI experiments, Δ[HbO<sub>2</sub>], Δ[HbR], and Δ[HbT] were higher than the baseline values, only Δ[HbO<sub>2</sub>] at an impact strength of 2.4 atm was lower than the baseline value.

The time courses of ΔICP and ΔCPP corresponding to different impact intensities are shown in Figures 4,5, respectively. Increasing impact strengths led to an increase in ΔICP. Moreover, the trend of change in ΔCPP corresponding to different impact strengths was like that of Δ[HbO<sub>2</sub>], Δ[HbR], and Δ[HbT]. For an impact strength of 2.4 atm, ΔCPP after TBI was almost lower than its baseline value. Table 2 shows the results of the average and standard deviation of ΔCPP, Δ[HbR], Δ[HbO<sub>2</sub>], and Δ[HbT] after TBI corresponding to different impact strengths and reveals the values of ΔCPP, Δ[HbR], Δ[HbO<sub>2</sub>], and Δ[HbT] decreased with increasing impacts.

The correlations between ΔCPP, and Δ[HbO<sub>2</sub>], Δ[HbR], and Δ[HbT] are shown in Figure 6. The relation between both ΔCPP and Δ[HbO<sub>2</sub>] (correlation =0.72) and Δ[HbT] (correlation =0.6) were significant (correlation =0.72), and the correlation between ΔCPP and Δ[HbR] was lower (correlation =0.36).

## Discussion

According to the results (Figures 2,3A), Δ[HbO<sub>2</sub>], Δ[HbR], and Δ[HbT] and ΔCPPs dropped immediately at the impact

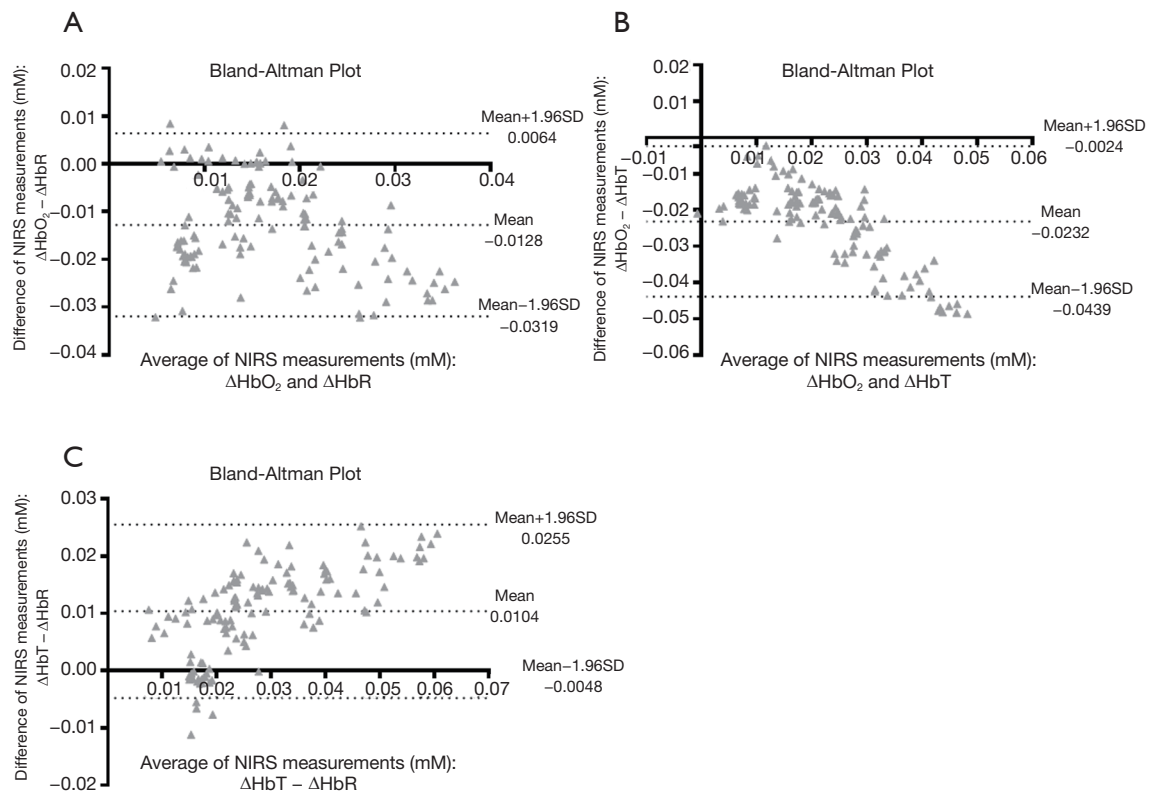


**Figure 2** Bland-Altman plot showing most of the measured differences were within the limits of agreement (LOA), mean difference  $\pm 1.96$  standard deviation (SD) of the difference. (A) Bland-Altman plot of the difference  $\{\Delta[\text{HbO}_2] - \Delta[\text{HbR}]\}$  and average of  $\Delta[\text{HbO}_2] - \Delta[\text{HbR}]$ . (B) Bland-Altman plot of the difference  $\{\Delta[\text{HbO}_2] - \Delta[\text{HbT}]\}$  and average of  $\Delta[\text{HbO}_2] - \Delta[\text{HbT}]$ . (C) Bland-Altman plot of the difference  $\{\Delta[\text{HbT}] - \Delta[\text{HbR}]\}$  and average of  $\Delta[\text{HbT}] - \Delta[\text{HbR}]$ . HbO<sub>2</sub>, oxy-hemoglobin; HbT, total-hemoglobin; HbR, deoxy-hemoglobin.

point and the  $\Delta\text{ICP}$  rose rapidly. This can be explained by the post-FPI apnea causing cerebral hypoxia and the distortion or displacement of the cerebral vasculature causing an increased ICP leading to a decrease in cerebral flow and cerebral hypoperfusion. The increased strength of trauma was associated with increasing  $\Delta\text{ICP}$  (17) and decreasing  $\Delta\text{CPP}$  at the impact point (*Figures 3A, 4A*, respectively).

Cerebral hyperperfusion can occur in the early stage of TBI (17), and this was seen in our  $\Delta\text{CPP}$  results (*Figure 4B*) where cerebral hyperperfusion occurred immediately after the TBI. Likewise, hyperemia following post-traumatic ischemia has been reported to occur due to metabolic demand by effective autoregulation (18), and this was also reflected in  $\Delta[\text{HbO}_2]$ ,  $\Delta[\text{HbR}]$ , and  $\Delta[\text{HbT}]$  after the FPI experiments in this study (*Figure 2*). At 1.6 to 2.4 atm of impact strength, the increasing  $\Delta\text{ICP}$  corresponded to decreases in  $\Delta\text{CPP}$ ,  $\Delta[\text{HbO}_2]$ ,  $\Delta[\text{HbR}]$ , and  $\Delta[\text{HbT}]$  (*Figure 3B* and *Table 1*). This can be explained by an

impairment in cerebral autoregulation, which saw the increasing ICP cause cerebral hypoperfusion (19,20) leading to a decrease in cerebral blood volume (21) and cerebral oxygenation (22), especially at 2.4 atm of impact strength. The values of  $\Delta[\text{HbR}]$  were all higher than  $\Delta[\text{HbO}_2]$  at 1.6, 2.0, and 2.4 atm. This can be explained by the injured brain cells needing more oxygenated hemoglobin to metabolize (23). Stocchetti *et al.* reported that increased CPP was positively correlated to cerebral oxygenation as it provides more oxygenated blood flow into the brain (24), and this is consistent with the present findings in the correlation between  $\Delta\text{CPP}$  and  $\Delta[\text{HbO}_2]$  (*Figure 5A*). The increases in  $\Delta\text{CPP}$  correlates with increases in brain oxygenation immediately after impact but may also imply disturbed autoregulation. The increase in CPP represents greater blood flow into the brain so the  $\Delta\text{CPP}$  was also positively correlated to  $\Delta[\text{HbT}]$ . The correlation between  $\Delta\text{CPP}$  and  $\Delta[\text{HbR}]$  was lower because deoxy-hemoglobin is associated with cell metabolism. The more injured

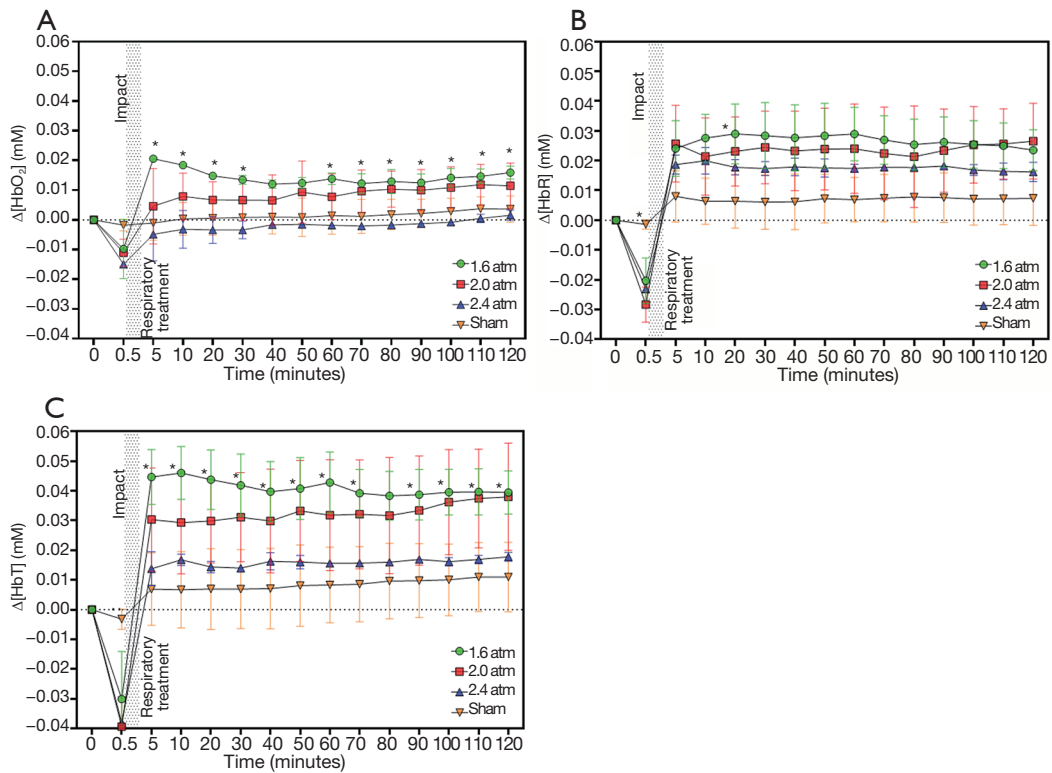


**Figure 3** Time courses of  $\Delta[\text{HbO}_2]$  (A),  $\Delta[\text{HbR}]$  (B),  $\Delta[\text{HbT}]$  (C) corresponding to different impact strengths. (A)  $\Delta[\text{HbO}_2]$  to different impact strength; (B)  $\Delta[\text{HbR}]$  to different impact strength; (C)  $\Delta[\text{HbT}]$  to different impact strength. \* indicates significance.  $\text{HbO}_2$ , oxy-hemoglobin; HbT, total-hemoglobin; HbR, deoxy-hemoglobin.

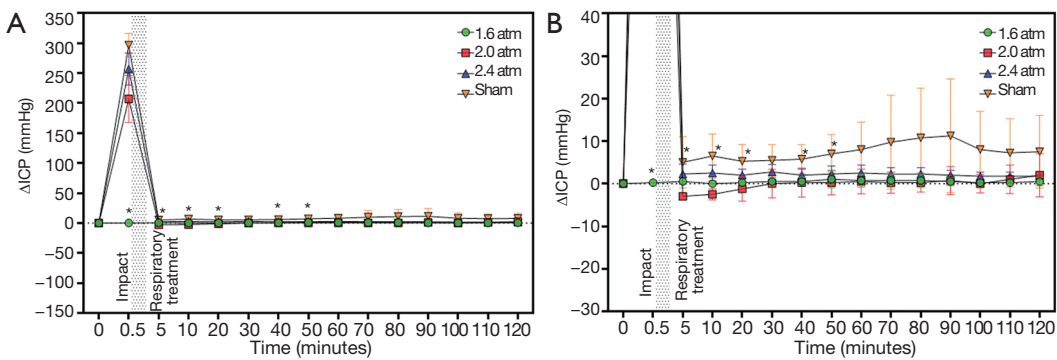


**Figure 4** Time courses of  $\Delta\text{ICP}$  (A) and  $\Delta\text{ICP}$  (B), after the impact point, corresponding to different impact strengths. (A) Time courses of  $\Delta\text{ICP}$  after the impact point by different impact strength; (B) time courses of  $\Delta\text{ICP}$  after the impact point by different impact strength with less scale. \* indicates significance. ICP, intracranial pressure.

brain cells require oxygen to metabolize, the more deoxy-hemoglobin is produced. Forcione *et al.* have nicely shown how this can be done with dynamic contrast-enhanced NIRS with indocyanine green in TBI patients (25,26).

The manner by which CBF can be measured has been established, including intravascular assessment, nuclear medicine ( $^{133}\text{Xe}$ ,  $^{85}\text{Kr}$ , and PET), thermodilution, ultrasound, and biomedical optics (27,28). However, this is

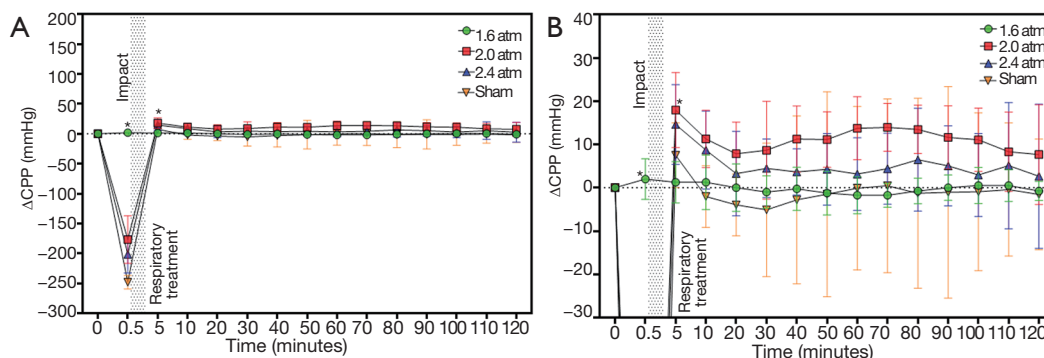


**Figure 5** Time courses of  $\Delta$ CPP (A) and  $\Delta$ CPP (B), after the impact point, corresponding to different impact strengths. (A) Time courses of  $\Delta$ CPP after the impact point by different impact strength; (B) time courses of  $\Delta$ CPP after the impact point by different impact strength with less scale. \* indicates significance. CPP, cerebral perfusion pressure.

**Table 2** The average and standard deviation of  $\Delta$ CPP,  $\Delta$ [HbO<sub>2</sub>],  $\Delta$ [HbR], and  $\Delta$ [HbT] after TBI corresponding with different impact strengths

Impact strength (atm)	$\Delta$ CPP (mmHg)	$\Delta$ HbO <sub>2</sub> (mM)	$\Delta$ HbR (mM)	$\Delta$ HbT (mM)
1.6	11.37±2.93	0.0145±0.0026	0.0267±0.0018	0.0411±0.0025
2.0	5.52±3.22	0.0087±0.0022	0.0239±0.0016	0.0326±0.0029
2.4	-0.99±2.97	-0.0018±0.0016	0.0177±0.0010	0.0158±0.0012

HbO<sub>2</sub>, oxy-hemoglobin; HbT, total-hemoglobin; HbR, deoxy-hemoglobin; ICP, intra-cranial pressure; CPP, cerebral perfusion pressure.

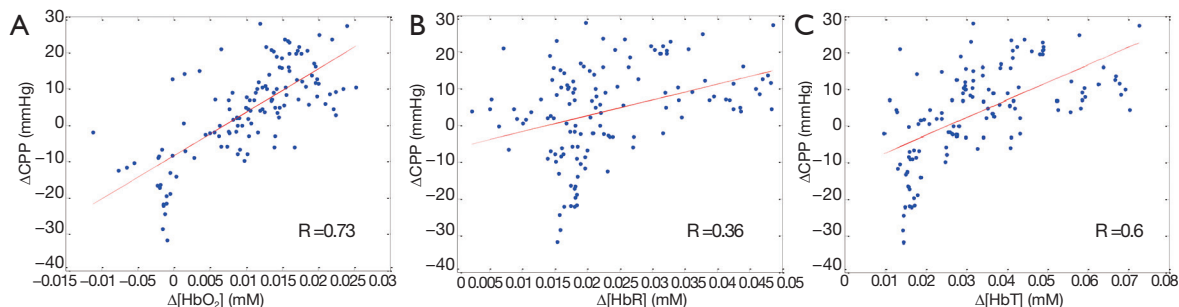


**Figure 6** Correlation between  $\Delta$ CPP and  $\Delta$ [HbO<sub>2</sub>] (A),  $\Delta$ [HbR] (B),  $\Delta$ [HbT] (C) after traumatic brain injury (TBI). (A) Correlation between  $\Delta$ CPP and  $\Delta$ [HbO<sub>2</sub>] after TBI; (B) correlation between  $\Delta$ CPP and  $\Delta$ [HbR] after TBI; (C) correlation between  $\Delta$ CPP and  $\Delta$ [HbT] after TBI. HbO<sub>2</sub>, oxy-hemoglobin; HbT, total-hemoglobin; HbR, deoxy-hemoglobin; CPP, cerebral perfusion pressure.

indirect evidence as  $\Delta$ [HbT] and  $\Delta$ CPP, are not identical to cerebral flow increase (29). Further survey is mandatory to clarify the relationship among the CBF, autoregulation, and NIRS parameters for applying this tool in clinical scenarios.

**Study limitation**

The major limitation of this study is its small sample size.

We also lack direct measurement of the CBF in different CPP, which may decrease the originality of the study. The overall correlation between CPP and NIRS parameters is not high, possibly because the CPP may also be impacted by variation of ICP after brain trauma. Any experimental study on TBI is as good as the animal model used to test a research hypothesis and in our study a fluid percussion model seemed appropriate for the qualitative evaluation of

CPP with NIRS. However further experiments on different injury models are warranted to confirm our findings.

## Conclusions

The results showed that  $\Delta$ CPP and  $\Delta$ [HbO<sub>2</sub>],  $\Delta$ [HbR], and  $\Delta$ [HbT] were inversely related to increased impact intensities. This data could be explained by the increase in ICP owing to increased impact intensities obstructing sufficient blood flow into the brain. In addition,  $\Delta$ [HbO<sub>2</sub>] and  $\Delta$ [HbT] were correlated to  $\Delta$ CPP positively. These results favor that the NIRS system may potentially assess cerebral ischemia and oxygenation non-invasively, and that changes of HbO<sub>2</sub> and HbT may be used to assess the level of CPP.

## Acknowledgments

This manuscript was edited by QIMS English editing services.

*Funding:* This research was partly supported by the Ministry of Science and Technology in Taiwan, under grants MOST 108-2221-E-009-054-MY2. This research was also partly supported by the Higher Education Sprout Project of the National Chiao Tung University and Ministry of Education (MOE), Taiwan.

## Footnote

*Conflicts of Interest:* All authors have completed the ICMJE uniform disclosure form (available at <http://dx.doi.org/10.21037/qims-20-777>). The authors have no conflicts of interest to declare.

*Ethical Statement:* All of the experimental procedures conformed to the guidelines of the National Institute of Health, and were approved by the Animal Care and Use Committee of Chi-Mei Medical Center (Affidavit of approval of Animal Use Protocol, Chi-Mei Medical Center, IACUC Approval No. 102120603) to minimize discomfort to the animals during the surgery and recovery periods.

*Open Access Statement:* This is an Open Access article distributed in accordance with the Creative Commons Attribution-NonCommercial-NoDerivs 4.0 International License (CC BY-NC-ND 4.0), which permits the non-commercial replication and distribution of the article with the strict proviso that no changes or edits are made and the original work is properly cited (including links to both the

formal publication through the relevant DOI and the license). See: <https://creativecommons.org/licenses/by-nc-nd/4.0/>.

## References

1. Gupta AK. Monitoring the injured brain in the intensive care unit. *J Postgrad Med* 2002;48:218-25.
2. Ganau M, Prisco L. Comment on "neuromonitoring in traumatic brain injury". *Minerva Anestesiologica* 2013;79:310-1.
3. Syrmos N, Ganau M, De Carlo A, Prisco L, Ganau L, Valadakis V, Grigoriou K, Iliadis C, Arvanitakis D. Dealing with the surgical and medical challenges of penetrating brain injuries. *Case Rep Surg* 2013;2013:209750.
4. Ganau M, Lavinio A, Prisco L. Delirium and agitation in traumatic brain injury patients: an update on pathological hypotheses and treatment options. *Minerva Anestesiologica* 2018;84:632-40.
5. Meixensberger J, Jaeger M, Vath A, Dings J, Kunze E, Roosen K. Brain tissue oxygen guided treatment supplementing ICP/CPP therapy after traumatic brain injury. *J Neurol Neurosurg Psychiatry* 2003;74:760-4.
6. Jaeger M, Soehle M, Schuhmann M, Winkler D, Meixensberger J. Correlation of continuously monitored regional cerebral blood flow and brain tissue oxygen. *Acta Neurochirurgica* 2005;147:51-6.
7. Friess SH, Ralston J, Eucker SA, Helfaer MA, Smith C, Margulies SS. Neurocritical care monitoring correlates with neuropathology in a swine model of pediatric traumatic brain injury. *Neurosurgery* 2011;69:1139-47.
8. Barazangi N, Hemphill III JC. Advanced cerebral monitoring in neurocritical care. *Neurology India* 2008;56:405-14.
9. Ferrari M, Giannini I, Sideri G, Zanette E. Continuous non invasive monitoring of human brain by near infrared spectroscopy. *Adv Exp Med Biol* 1985;191:873-82.
10. Wyatt JS, Cope M, Delpy DT, Wray S, Reynolds EO. Quantification of cerebral oxygenation and haemodynamics in sick newborn infants by near infrared spectrophotometry. *Lancet* 1986;2:1063-6.
11. Hasan S, Chari A, Ganau M, Uff C. Defining New Research Questions and Protocols in the Field of Traumatic Brain Injury through Public Engagement: Preliminary Results and Review of the Literature. *Emerg Med Int* 2019;2019:9101235.
12. Ganau M, Iqbal M, Ligarotti GKI, Syrmos N. Breakthrough in the assessment of cerebral perfusion and vascular permeability after brain trauma through the adoption of dynamic indocyanine green-enhanced

- near-infrared spectroscopy. *Quant Imaging Med Surg* 2020;10:2081-4.
13. Kuo JR, Lin BS, Cheng CL, Chio CC. Hypoxic-state estimation of brain cells by using wireless near-infrared spectroscopy. *IEEE J Biomed Health Inform* 2014;18:167-73.
  14. Delpy DT, Cope M, van der Zee P, Arridge S, Wray S, Wyatt J. Estimation of optical pathlength through tissue from direct time of flight measurement. *Phys Med Biol* 1988;33:1433-42.
  15. Ferrari M, Cettolo V, Quaresima V. Light source-detector spacing of near-infrared-based tissue oximeters and the influence of skin blood flow. *J Appl Physiol* (1985) 2006;100:1426; author reply 1427.
  16. McIntosh TK, Vink R, Noble L, Yamakami I, Fernyak S, Soares H, Faden AL. Traumatic brain injury in the rat: characterization of a lateral fluid-percussion model. *Neuroscience* 1989;28:233-44.
  17. Werner C, Engelhard K. Pathophysiology of traumatic brain injury. *Br J Anaesth* 2007;99:4-9.
  18. Carlson BE, Arciero JC, Secomb TW. Theoretical model of blood flow autoregulation: roles of myogenic, shear-dependent, and metabolic responses. *Am J Physiol Heart Circ Physiol* 2008;295:H1572-9.
  19. Frank JI. Large hemispheric infarction, deterioration, and intracranial pressure. *Neurology* 1995;45:1286-90.
  20. Grubb RL Jr, Raichle ME, Phelps ME, Ratcheson RA. Effects of increased intracranial pressure on cerebral blood volume, blood flow, and oxygen utilization in monkeys. *J Neurosurg* 1975;43:385-98.
  21. Kobari M, Gotoh F, Tomita M, Tanahashi N, Shinohara T, Terayama Y, Mihara B. Bilateral hemispheric reduction of cerebral blood volume and blood flow immediately after experimental cerebral hemorrhage in cats. *Stroke* 1988;19:991-6.
  22. Johnston AJ, Steiner LA, Coles JP, Chatfield DA, Fryer TD, Smielewski P, Hutchinson PJ, O'Connell MT, Al-Rawi PG, Aigbirihio FI, Clark JC, Pickard JD, Gupta AK, Menon DK. Effect of cerebral perfusion pressure augmentation on regional oxygenation and metabolism after head injury. *Crit Care Med* 2005;33:189-95; discussion 255-7.
  23. Marchal G, Young AR, Baron JC. Early postischemic hyperperfusion: pathophysiologic insights from positron emission tomography. *J Cereb Blood Flow Metab* 1999;19:467-82.
  24. Stocchetti N, Chiericato A, De Marchi M, Croci M, Benti R, Grimoldi N. High cerebral perfusion pressure improves low values of local brain tissue O<sub>2</sub> tension (PtiO<sub>2</sub>) in focal lesions. *Acta Neurochir Suppl* 1998;71:162-5.
  25. Forcione M, Yakoub KM, Chiarelli AM, Perpetuini D, Merla A, Sun R, Sawosz P, Belli A, Davies DJ. Dynamic contrast-enhanced near-infrared spectroscopy using indocyanine green on moderate and severe traumatic brain injury: a prospective observational study. *Quant Imaging Med Surg* 2020;10:2085-97.
  26. Forcione M, Chiarelli AM, Davies DJ, Perpetuini D, Sawosz P, Merla A, Belli A. Cerebral perfusion and blood-brain barrier assessment in brain trauma using contrast-enhanced near-infrared spectroscopy with indocyanine green: A review. *J Cereb Blood Flow Metab* 2020;40:1586-98.
  27. Shepelytskyi Y, Hane FT, Grynko V, Li T, Hassan A, Albert MS. Hyperpolarized <sup>129</sup>Xe Time-of-Flight MR Imaging of Perfusion and Brain Function. *Diagnostics (Basel)* 2020;10:630.
  28. Adjedj J, Picard F, Vanhaverbeke M, De Bruyne B, Cariou A, Wu M, Janssens S, Varenne O. A novel approach to assess cerebral and coronary perfusion after cardiac arrest. *Intensive Care Med* 2018;6:39.
  29. Fantini S, Sassaroli A, Tgavalekos KT, Kornbluth J. Cerebral blood flow and autoregulation: current measurement techniques and prospects for noninvasive optical methods. *Neurophotonics* 2016;3:031411.

**Cite this article as:** Huang YK, Lin CK, Wang CC, Kuo JR, Lai CF, Chen CW, Lin BS. A novel wireless optical technique for quantitative evaluation of cerebral perfusion pressure in a fluid percussion animal model of traumatic brain injury. *Quant Imaging Med Surg* 2021;11(6):2388-2396. doi: 10.21037/qims-20-777

## A. Implementation of wireless multi-channel near-infrared spectroscopy (NIRS) system

A wireless multi-channel near infrared spectroscopy system was designed and implemented to continuously monitor the relative concentrations of oxy-hemoglobin (HbO<sub>2</sub>) and deoxy-hemoglobin (HbR) under traumatic brain injury. The system architecture of the wireless multi-channel NIRS system, which includes a wireless signal acquisition module, a NIRS probe, and a host system. The NIRS probe consists of light emitting diodes (LEDs) and photodiodes (PDs). LED is used to provide red and infrared light sources, and PD is used to detect and convert the diffusely reflected lights into electrical signals. The wireless signal acquisition module was designed to drive the red and infrared lights of LEDs and receive the signal from PDs. When LED emits the light to pass through the biological tissue, most of light will be diffused rapidly due to scattering, and part of light will be absorbed by the tissue, especially HbO<sub>2</sub> and HbR which are mainly absorbers in the region of near infrared wavelength. In general, the mean path of light is like a banana shaped, and the maximum penetrating depth is about a half of the separating distance between the light source and the detector. Then, the diffusely reflected light detected by photodiodes will be delivered into the wireless signal acquisition module, and be amplified, filtered, digitized and transmitted wirelessly to the host system.

### Probe

The LED and photodiode used in the NIRS probe are SMT735/850 (EPITEX, Japan) and PD15-22C/TR8 (EVERLIGHT, Taiwan) respectively. The used LED is a dual-wavelength LED (red and infrared lights), and its light intensity is about 0.3 mW. The distance between LED and PD is about 1.6 cm. In order to contact closely with rat's head, the substrate of the NIRS probe was made of flexible black rubber. And the rubber tape with Velcro hook and loop is used to tie on rat's head to help hold the probe.

### Wireless signal acquisition module

The wireless signal acquisition module is mainly consisting of a LED driving circuits, a front-end amplifier circuits, a microcontroller, and a wireless transmission circuit. The LED driving circuits include a multiplexer, operation amplifiers, and NPN transistors. The multiplexer controlled by the microcontroller is used to turn the LED on or off. The operation amplifiers are used to provide the emitter of NPN transistors the stable bias to ensure constant current through these LEDs. The front-end amplifier circuits are made up of trans-impedance amplifiers and low-pass filters. The trans-impedance amplifier with the gain of  $2 \times 10^7$  V/A, was designed to convert the PD current signal into the voltage signal. And the cut-off frequency of the low-pass filter was set to 0.5 kHz. Then, a 12-bit analog-to-digital converter (ADC) built in the microcontroller will digitize the amplified PD signal with the sampling rate of 25 Hz. The microcontroller is used to control ADC and wireless transmission circuit, and calculate NIRS parameters, such as  $\Delta[\text{HbO}_2]$ ,  $\Delta[\text{HbR}]$ , and  $\Delta[\text{HbT}]$ . Finally, the digitized PD signals and the calculated NIRS parameters will be sent to the wireless transmission circuit. The wireless transmission circuit composed of a printed circuit board (PCB) antenna and a Bluetooth module which is fully compliant with the Bluetooth v2.0+ EDR specification.

### Host system

In this study, a laptop was used as the platform of the host system, and the operation system of the host system is Windows 7. The NIRS parameter monitoring program built in the host system was developed on Microsoft Visual C#. The program provides the functions of receiving data from the wireless signal acquisition module, real-time signal display and data storage.

## B. Theoretical models of tissue optics

The variation in the concentrations of HbO<sub>2</sub> and HbR can be quantified by using modified Beer-lambert law (MBLL) (14,15). MBLL is an empirical equation of optical attenuation in a highly scattering medium. The variation in the concentration of absorber will cause the change of optical intensity, and the relationship between the absorber's concentration and the optical intensity can be expressed as

$$\Delta OD = -\log \frac{I_f}{I_i} = \Delta \mu_a BL \quad [1]$$

where  $\Delta OD$  is the variation of the optical density, and  $I_f$  and  $I_i$  are the detected intensities of the diffusely reflected light before and after the concentration change respectively. The parameter  $B$ , named the differential path length factor (DPF), is a correction factor related to the average light traveling pathway between light source and detector.  $L$  denotes the distance between the light source and the detector. And  $\Delta \mu_a$  denotes the change of absorption coefficient of the tissue. In the infrared wavelength (from 700 to 900 nm), HbO<sub>2</sub> and HbR are most significant absorbers in the biological tissue. Thus,  $\Delta \mu_a$  can be simplified as

$$\Delta \mu_a = \varepsilon_{\text{HbO}_2} \Delta[\text{HbO}_2] + \varepsilon_{\text{HbR}} \Delta[\text{HbR}] \quad [2]$$

Here,  $\varepsilon_{\text{HbO}_2}$  and  $\varepsilon_{\text{HbR}}$  denote the extinction coefficients of HbO<sub>2</sub> and HbR respectively.  $\Delta[\text{HbO}_2]$  and  $\Delta[\text{HbR}]$  are the variations in the concentrations of HbO<sub>2</sub> and HbR respectively. Then the Equation [1] corresponding to specific wavelength  $\lambda$  can be rewritten as

$$\Delta OD^\lambda = (\varepsilon_{\text{HbO}_2}^\lambda \Delta[\text{HbO}_2] + \varepsilon_{\text{HbR}}^\lambda \Delta[\text{HbR}]) B^\lambda L \quad [3]$$

Next, the variations in the concentrations of HbO<sub>2</sub> and HbR can be solved by using the change of the optical intensity

corresponding to two or more different wavelengths. The solution of  $\Delta[\text{HbO}_2]$  and  $\Delta[\text{HbR}]$  can be expressed as

$$\Delta[\text{HbO}_2] = (\varepsilon_{\text{HbR}}^{\lambda_1} \frac{\Delta OD^{\lambda_2}}{B^{\lambda_2}} - \varepsilon_{\text{HbR}}^{\lambda_2} \frac{\Delta OD^{\lambda_1}}{B^{\lambda_1}}) / (\varepsilon_{\text{HbR}}^{\lambda_1} \varepsilon_{\text{HbO}_2}^{\lambda_2} - \varepsilon_{\text{HbR}}^{\lambda_2} \varepsilon_{\text{HbO}_2}^{\lambda_1}) L \quad [4]$$

$$\Delta[\text{HbR}] = (\varepsilon_{\text{HbO}_2}^{\lambda_2} \frac{\Delta OD^{\lambda_1}}{B^{\lambda_1}} - \varepsilon_{\text{HbO}_2}^{\lambda_1} \frac{\Delta OD^{\lambda_2}}{B^{\lambda_2}}) / (\varepsilon_{\text{HbR}}^{\lambda_1} \varepsilon_{\text{HbO}_2}^{\lambda_2} - \varepsilon_{\text{HbR}}^{\lambda_2} \varepsilon_{\text{HbO}_2}^{\lambda_1}) L \quad [5]$$

Here, the wavelengths of  $\lambda_1$  and  $\lambda_2$  used in this study are 735 and 850 nm respectively. And assuming that the biological tissue is a semi-infinite medium, the parameter  $B$  can be given by

$$B = \frac{1}{2} \left( \frac{3\mu'_s}{\mu_a^{\text{initial}}} \right)^{1/2} \left[ 1 - \frac{1}{1 + L(3\mu'_s \mu_a^{\text{initial}})^{1/2}} \right] \quad [6]$$

where  $\mu'_s$  is the reduced scattering coefficient,  $\mu_a^{\text{initial}}$  is the initial absorption coefficient, and  $\mu_s^{\text{initial}}$  is initial scattering coefficient. In this study, the concentration changes of total-hemoglobin  $\{\Delta[\text{HbT}]\}$  is defined as

$$\Delta[\text{HbT}] = \Delta[\text{HbO}_2] + \Delta[\text{HbR}] \quad [7]$$

### C. Experiments for traumatic brain injury rat models

#### *Animals preparation*

Adult male Sprague-Dawley rats weighing  $375 \pm 25$  g were prepared in the experiment. All rats were reared on a 12-hour light/12-hour dark cycle, and allowed to access to food and water freely. All experimental procedures were conformed to the guidelines of National Institute of Health, Taiwan, and were approved by Animal Care and Use Committee of Chi-Mei Medical Center to minimize discomfort to animals during surgery and recovery periods. All rats (number of rats =16) were randomly assigned to four impacts (sham, 1.6, 2.0, and 2.4 atm), and monitored by the wireless NIRS system, ICP and MAP. All rats were anesthetized with sodium pentothal (25 mg/kg, i.p.; Sigma Chemical Co., St Louis, MO, USA) and a mixture containing ketamine (44 mg/kg, i.m.; Nan Kuang Pharmaceutical, Tainan, Taiwan), atropine (0.02633 mg/kg, i.m.; Sintong Chemical Industrial Co., Ltd., Taoyuan, Taiwan), and xylazine (6.77 mg/kg, i.m.; Bayer, Leverkusen, Germany). All rats would be sacrificed in the third day post-surgery.

#### *Experiment design for traumatic brain injury*

In this study, fluid percussion injury (FPI) model was used to reproduce TBI in the rats (16). Before FPI experiment, the rat was anesthetized first. And then its head was placed in a stereotaxic frame, and its ears was inserted by ear bars to tight its head. In order to keep the rat core temperature at 37 °C, a rectal temperature probe attached to the thermostatic controller was inserted into the rat's colon. Next, the fur on the rat head was trimmed, and the scalp was incised sagittally. Afterwards, a circular craniotomy on the skull was drilled to set the impact point which was located at the anterior-posterior -3 mm and lateral +4 mm from the bregma. The leur-lock connector connected with a sealed and fluid-filled reservoir was secured into the craniotomy (Figure S1).

After that, the monitoring devices, such as the wireless NIRS system, ICP, and MAP, were installed and began to monitor for 2 hours. Then, a pendulum struck the reservoir to generate a fluid wave to impact the rat brain, and a respiratory treatment procedure was carried out to help rat's respiration immediately after FPI experiment. Finally, after all the experiment finished, the monitoring device, connector and acrylic were removed from the rat, and the incisions were sutured.

The mainly monitoring position of NIRS probe was focus at striatum region of rat's brain, and maximum penetrating depth was about 8 mm which located at anterior-posterior -0.5 mm and lateral +3.5 mm from bregma (Figure S2). In this study, the changes of 30-second  $\text{HbO}_2$  and  $\text{HbR}$  were recorded as the data baseline before the FPI experiment.

In order to measure the mean arterial blood pressure, the right femoral artery was cannulated with polyethylene tubing, and a 3-way stopcock connected with the pressure transducer and the data acquisition system (PowerLab/8sp, ADInstruments) were also used. In addition, a pressure-monitoring catheter of ICP monitor (Codman ICP Express Monitor, Codman & Shurtleff, Inc.) was located at anterior-posterior -0.8 mm and lateral +4 mm from the bregma and was installed on the stereotaxic frame. When the experiment began, the data of MAP and ICP would be recorded as the baseline first. Thereafter MAP and ICP values would be recorded every 10 minutes.

In order to monitor the short-term changes of MAP and ICP, the data during impact and 4.5 minutes after impact were also recorded. Figure S3 shows the location of the NIRS probe, the ICP catheter, and the leur-lock connector.

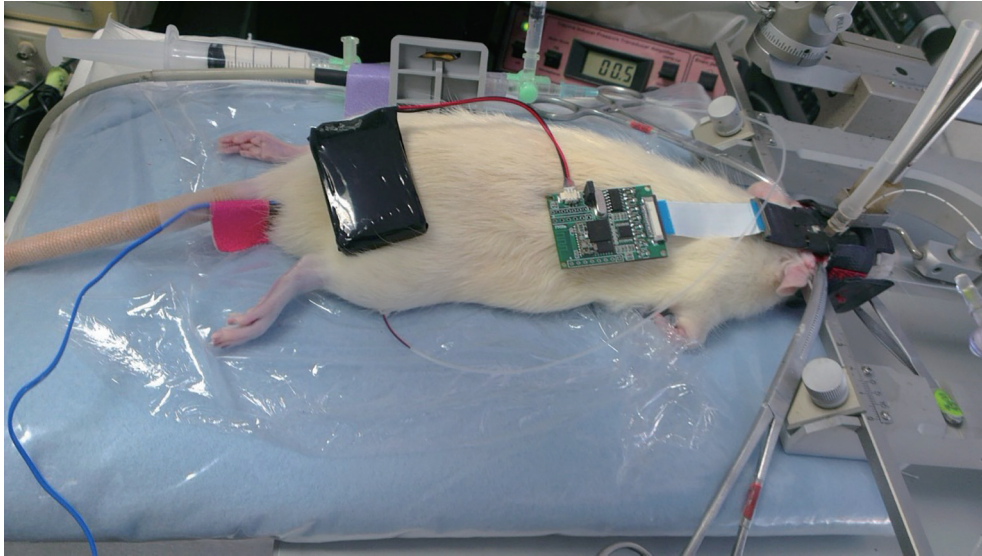


**Figure S1** Mice setting.



**Figure S2** Experiment equipment grossly during recording.

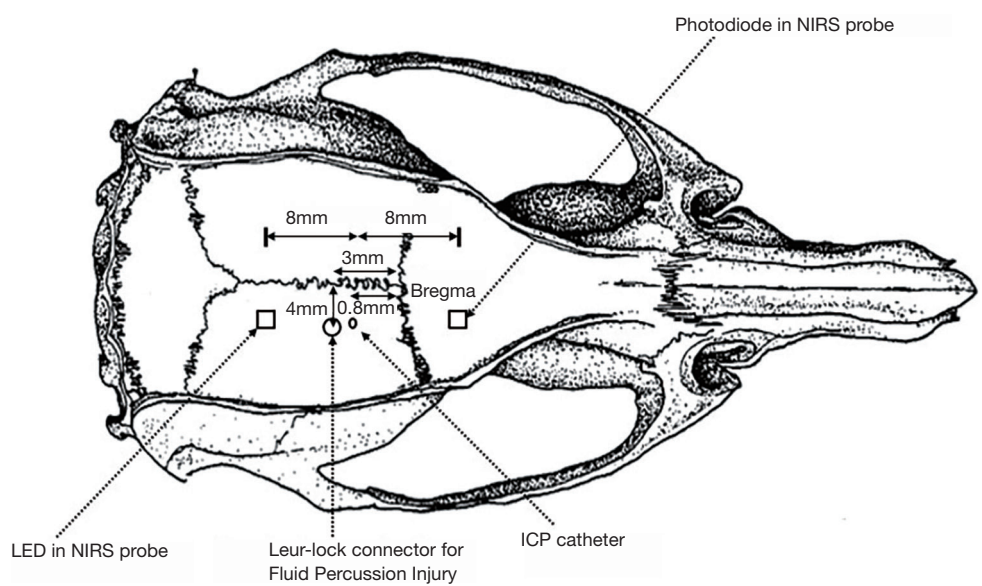


**Figure S3** Anatomic position on the skull. NIRS, near-infrared spectroscopy; LED, light emitting diode; ICP, intracranial pressure.